Electronic Supplementary Material (ESI) for RSC Chemical Biology.

SUPPORTING INFORMATION

Dynamic visualization of type II peptidyl carrier protein recognition in pyoluteorin biosynthesis

Joshua C. Corpuz[a], Larissa M. Podust[b], Tony D. Davis[a], Matt J. Jaremko[a], Michael D. Burkart*[,†]

[a] *Department of Chemistry and Biochemistry, University of California-San Diego, 9500 Gilman Drive, La Jolla, CA 92093-0358, USA*

[b] *Skaggs School of Pharmacy and Pharmaceutical Sciences, University of California-San Diego, 9500 Gilman Dr., La Jolla, CA 92093-0755, USA.*

*Correspondence should be directed to mburkart@ucsd.edu.

A. Synthesis of prolyl-adenosine vinylsulfonamide probe

Chemical reagents were purchased from Acros, Fluka, Sigma-Aldrich, or TCI. Deuterated NMR solvents were purchased from Cambridge Isotope Laboratories. All reactions were conducted with vigorously dried anhydrous solvents that were obtained by passing through a solvent column exposed of activated A2 alumina. All reactions were performed under positive pressure of argon in flame-dried glassware sealed with septa and stirred with Teflon coated stir bars using an IKAMAG TCT-basic mechanical stirrer (IKA GmbH). Analytical Thin Layer Chromatograpy (TLC) was performed on Silica Gel 60 F254 precoated glass plates (EM Sciences). Visualization was achieved with UV light and/or appropriate stain (I_2 on SiO_2, $KMnO_4$, bromocresol green, dinitrophenylhydrazine, ninhydrin, or ceric ammonium molybdate). Flash column chromatography was carried out with Geduran Silica Gel 60 (40–63 mesh) from EM Biosciences. Yield and characterization data correspond to isolated, chromatographically, and spectroscopically homogeneous materials. ^{1}H NMR spectra were recorded on Varian Mercury 400, Varian Mercury Plus 400, or JEOL ECA500 spectrometers. ^{13}C NMR spectra were recorded at 100 MHz on Varian Mercury 400 or Varian Mercury Plus 400 spectrometers. Chemical shifts for ^{1}H NMR and ^{13}C NMR analyses were referenced to the reported values of Gottlieb (1) using the signal from the residual solvent for ^{1}H spectra, or to the ^{13}C signal from the deuterated solvent. Chemical shift δ values for the ^{1}H and ^{13}C spectra are reported in parts per millions (ppm) relative to these referenced values, and multiplicities are abbreviated as s=singlet, d=doublet, t=triplet, q-quartet, m=multiplet, b=broad. All ^{13}C NMR spectra were recorded with complete proton decoupling. FID files were processed using MestreNova 10.0 (MestreLab Research). Electrospray ionization (ESI) mass spectrometric analyses were preformed using a ThermoFinnigan LCQ Deca spectrometer. Spectral data and procedures are provided for all new compounds and copies of spectra have been provided.

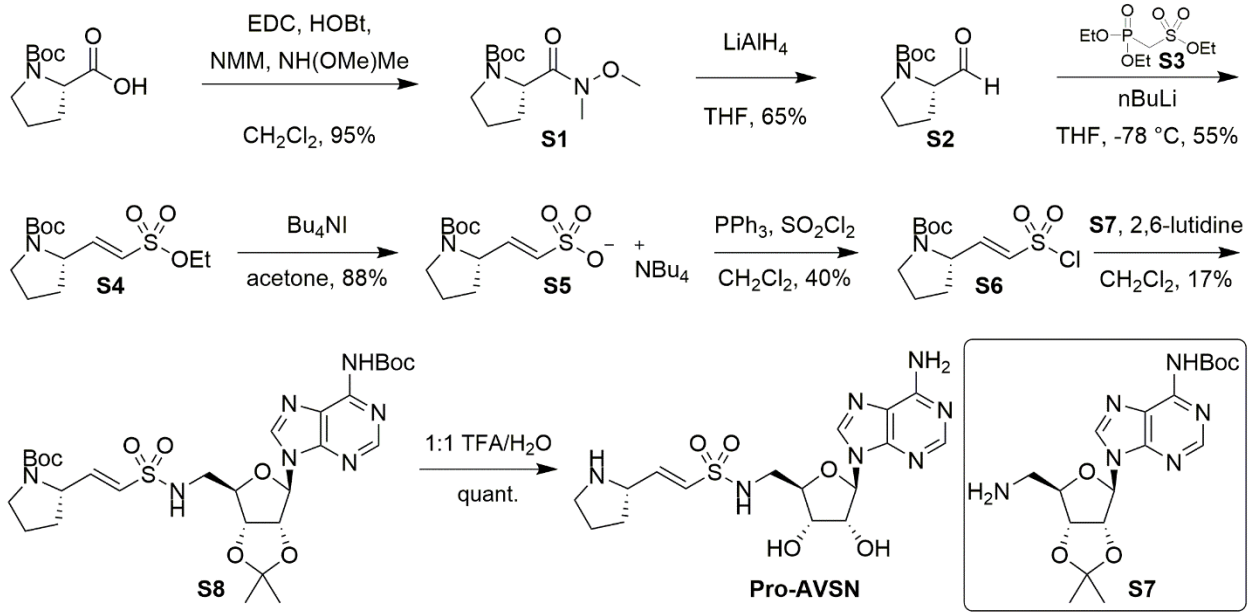

Scheme S1: Synthesis of prolyl-adenosine vinylsulfonamide (Pro-AVSN). EDC=1-Ethyl-3-(3-dimethylaminopropyl)carbodiimide); HOBt=hydroxybenzotriazole; NMM=*N*-methylmorpholine; TFA=trifluoroacetic acid.

tert-butyl (S)-2-(methoxy(methyl)carbamoyl)pyrrolidine-1-carboxylate (S1). In a 250 mL round-bottom flask, *N*-Boc-L-proline (5.11 g, 23.7 mmol, 1.0 equiv.) and 100 mL CH_2Cl_2 were added. The vessel was cooled to 0 °C before the addition of HOBt (3.54 g, 26.2 mmol, 1.1 equiv.) and EDC•HCl (5.50 g, 28.7 mmol, 1.2 equiv.). The reaction was stirred for 20 minutes at 0 °C

before the addition of *N*,*O*-dimethylhydroxylamine-hydrochloride (2.69 g, 27.6 mmol, 1.2 equiv.) and 4-methylmorpholine (3.0 mL, 27.3 mmol, 1.2 equiv.). The reaction was warmed to room temperature and stirred overnight. After 14 h, the volatiles were removed by rotary evaporation and the resulting residue was dissolved in EtOAc (250 mL) and washed with 1 N HCl (2x50 mL), saturated $NaHCO_3$ (50 mL), and brine (50 mL). The organic phase was dried ($MgSO_4$), filtered, and concentrated by rotary evaporation. Purification by silica flash chromatography (1:1 hexanes/diethyl ether → diethyl ether) afforded Weinreb amide **S1** (5.81 g, 95%) as a clear viscous oil.
TLC: R_f 0.57 (diethyl ether). **^{1}H-NMR** (400 MHz, $CDCl_3$): δ4.58 (dd, *J* = 39.3, 8.7, 3.4 Hz, 1H), 3.71 (s, 2H), 3.65 (s, 1H), 3.55–3.44 (m, 1H), 3.44–3.29 (m, 1H), 3.12 (s, 3H), 2.22–2.03 (m, 1H), 1.98–1.86 (m, 1H), 1.85–1.71 (m, 2H), 1.38 (s, 5H), 1.34 (s, 4H). **^{13}C-NMR** (100 MHz, $CDCl_3$): δ 154.50, 153.92, 79.62, 61.28, 56.83, 46.88, 32.42, 30.49, 29.61, 28.48, 24.05, 23.40. **HR-ESI-MS** *m/z* calcd. $[C_{12}H_{22}N_2O_4Na]^+$: 281.1472, found 281.1469.

tert-butyl (S)-2-formylpyrrolidine-1-carboxylate (S2). In a 200 mL pear-shaped flask, *N*-Boc-L-proline Weinreb amide **S1** (2.02 g, 7.81 mmol, 1.0 equiv.) and 100 mL THF were added. The vessel was cooled to 0 °C before the addition of $LiAlH_4$ (387.4 mg, 10.2 mmol, 1.3 equiv.). After stirring for 1 h at 0 °C, the reaction was quenched by the slow, dropwise addition of an aqueous solution of 1.5 M $NaHSO_4$ (25 mL) and saturated Rochelle's salt (25 mL). The aqueous phase was extracted with EtOAc (3x50 mL) and the combined organic extracts were washed with saturated $NaHCO_3$ (50 mL), water (50 mL), and brine (50 mL). The organic phase was dried ($MgSO_4$), filtered, and concentrated by rotary evaporation to afford aldehyde **S2** (1.56 g, quant.) as a clear liquid that was carried forward without additional purification.
TLC: R_f 0.55 (1:1 hexanes/EtOAc). **^{1}H-NMR** (400 MHz, $CDCl_3$): δ 9.56 (s, 0.5 H), 9.45 (s, 0.5 H), 4.10–4.00 (m, 1H), 3.61–3.49 (m, 1H), 3.45–3.31 (m, 1H), 2.19–2.05 (m, 1H), 2.05–1.93 (m, 1H), 1.91–1.79 (m, 2H), 1.47 (s, 5H), 1.42 (s, 4H).**ESI-MS** m/z (rel int): (pos) 254.07 ($[M+MeOH+Na]^+$, 100); 222.04 ($[M+Na]^+$, 25). **HR-ESI-MS** *m/z* calcd. $[C_{10}H_{17}NO_3Na]^+$: 222.1101, found 222.1102.

***tert*-butyl (*S*,*E*)-2-(2-(ethoxysulfonyl)vinyl)pyrrolidine-1-carboxylate (S4).** In a 50 mL pear-shaped flask, ethyl(diethoxyphosphoryl)methane sulfonate **S3** (2) (2.12 g, 8.13 mmol, 1.2 equiv.) and 16 mL THF were added. The vessel was cooled to -78 °C before the dropwise addition of *n*BuLi (5.5 mL of 1.6 M solution in hexanes, 8.81 mmol. 1.3 equiv.). Stirring was continued for 1 h at -78 °C. In a separate 100 mL round-bottom flask, aldehyde **S2** (1.36 g, 6.77 mmol, 1.0 equiv.) and 45 mL THF were added and the flask was cooled to -78 °C for 1 h. The phosphonate carbanion solution was cannulated into the solution containing **S2**. After stirring for 4 h at -78 °C, the reaction was quenched by the addition of H_2O (50 mL) and the volatiles were removed by rotary evarporation. The resulting aqueous phase was extracted with CH_2Cl_2 (3x50 mL) and the combined organic extracts were dried ($MgSO_4$), filtered, and concentrated by rotary evaporation. Purification by silica flash chromatography (3:2 hexanes/diethyl ether) afforded ethyl vinyl sulfonate ester **S4** (1.36 g, 55%) as a white solid.
TLC: R_f 0.54 (1:1 hexanes/EtOAc). **^{1}H-NMR** (400 MHz, $CDCl_3$): δ 6.75 (dd, *J* = 15.0, 5.7 Hz, 1H), 6.18 (d, *J* = 15.0 Hz, 1H), 4.44 (d, *J* = 22.2 Hz, 1H), 4.21–4.09 (m, 2H), 3.48–3.33 (m, 2H), 1.94–1.74 (m, 4H), 1.41 (s, 5H), 1.36 (bs, 3H). **^{13}C-NMR** (100 MHz, $CDCl_3$): δ 148.57, 124.30, 57.26, 46.77, 31.58, 30.65, 28.43, 23.79, 22.95, 14.86. **ESI-MS** m/z (rel int): (pos) 327.99($[M+Na]^+$, 100); 322.91 ($[M+NH_4]^+$, 30). **HR-ESI-MS** *m/z* calcd. $[C_{13}H_{23}NO_5SNa]^+$: 328.1189, found 328.1187; $[C_{13}H_{23}NO_5SNH_4]^+$: 323.1635, found 323.1634.

***tert*-butyl (*S*,*E*)-2-(2-(chlorosulfonyl)vinyl)pyrrolidine-1-carboxylate (S6).** In a 100 mL round-bottom flask, ethyl vinyl sulfonate ester **S4** (255.6 mg, 0.8370 mmol, 1.0 equiv) and tetrabutylammonium iodide (410.1 mg, 1.1103 mmol, 1.3 equiv.) were dissolved in 17 mL acetone. The mixture was refluxed for 40 h. The volatiles were removed by rotary evaporation

and the residue was dissolved in CH_2Cl_2 (50 mL) and washed with H_2O (2x10 mL). The organic extracts were dried ($MgSO_4$), filtered, and concentrated by rotary evaporation to afford crude vinyl sulfonate tetrabutylammonium salt **S5**, which was carried forward without additional purification.

In a 25 mL pear-shaped flask, triphenylphosphine (443.6 mg, 1.6913 mmol, 2.0 equiv.) was dissolved in 5 mL CH_2Cl_2 and cooled to 0 °C. To the flask was added sulfuryl chloride (0.15 mL, 1.8504 mmol, 2.2 equiv.), followed by a solution of crude vinyl sulfonate tetrabutylammonium salt **S5** in 5 mL CH_2Cl_2. The mixture was stirred at 0 °C for 3 h, then the volatiles were removed by rotary evaporation. Purification by silica flash chromatography (9:1 → 1:1 hexanes/EtOAc) afforded vinyl sulfonyl chloride **S6** (98.8 mg, 40%, 2 steps) as a brown solid.
TLC: R_f 0.29 (3:1 hexanes/EtOAc). **^{1}H-NMR** (400 MHz, $CDCl_3$): δ 6.99–6.89 (m, 1H), 6.71 (d, *J* = 13.9 Hz, 1H), 4.47 (bs, 1H), 3.47 (bs, 2H), 2.20 (bs, 1H), 1.99–1.77 (m, 4H), 1.44 (s, 9H). **^{13}C-NMR** (100 MHz, $CDCl_3$): δ 149.45, 133.18, 57.00, 46.72, 31.57, 28.44, 23.15. **HR-ESI-MS** *m/z* calcd. $[C_{11}H_{18}ClNO_4SNa]^+$: 318.0537, found 318.0538.

***tert*-butyl (*S*)-2-((*E*)-2-(*N*-(((3a*R*,4*R*,6*R*,6a*R*)-6-(6-((*tert*-butoxycarbonyl)amino)-9H-purin-9-yl)-2,2-dimethyltetrahydrofuro[3,4-d][1,3]dioxol-4-yl)methyl)sulfamoyl)vinyl)pyrrolidine-1-carboxylate (Boc-Pro-AVSN[N^6-Boc-2′,3′-isopropylidene adenosine]; S8).** In a 10 mL pear-shaped flask, N^6-Boc-2′,3′-isopropylidene 5′-aminodeoxyladenosine (*tert*-butyl (9-((3aR,4R,6R,6aR)-6-(aminomethyl)-2,2-dimethyltetrahydrofuro[3,4-d][1,3]dioxol-4-yl)-9H-purin-6-yl)carbamate) **S7** (3) (73.2 mg,0.1801 mmol, 1.0 equiv.) and 2,6,-lutidine (60 µL, 0.5180 mmol, 2.9 equiv.) were dissolved in 2 mL CH_2Cl_2. To the clear solution was added vinyl sulfonyl chloride **S6** (53.7 mg, 0.1816 mmol, 1.0 equiv.) as a solution in 2 mL CH_2Cl_2. After stirring for 3 h at r.t. (21 °C), the volatiles were removed by rotary evaporation. Purification by silica flash chromatography (1:1 hexanes/EtOAc → EtOAc) afforded protected vinyl sulfonamide Boc-Pro-AVSN [N^6-Boc-2′,3′-isopropylidene] **S8** (20.7 mg, 17%) as a white solid.
TLC: R_f 0.39 (EtOAc). **^{1}H-NMR** (400 MHz, $CDCl_3$): δ 8.82 (s, 1H), 7.99 (s, 1H), 6.59 (dt, *J* = 14.5, 8.3 Hz, 1H), 6.17 (t, *J* = 13.6 Hz, 1H), 5.84 (d, *J* = 4.8 Hz, 1H), 5.33–5.29 (m, 1H), 5.17–5.09 (m, 1H), 4.56 (d, *J* = 20.1 Hz, 1H), 3.50–3.28 (m, 4H), 2.17–2.05 (m, 1H), 1.91–1.82 (m, 4H), 1.80–1.74 (m, 2H), 1.62 (s, 3H), 1.57 (s, 7H), 1.39 (s, 4H), 1.36 (s, 3H). **^{13}C-NMR** (100 MHz, $CDCl_3$): δ 153.12, 144.83, 142.00, 127.73, 123.06, 93.54, 83.14, 82.49, 81.69, 31.72, 31.01, 28.47, 28.23, 27.59, 25.33. **HR-ESI-MS** *m/z* calcd. $[C_{29}H_{44}N_7O_9S]^+$: 666.2916, found 666.2908.

(*E*)-*N*-(((2*R*,3*S*,4*R*,5*R*)-5-(6-amino-9H-purin-9-yl)-3,4-dihydroxytetrahydrofuran-2-yl)methyl)-2-((*S*)-pyrrolidin-2-yl)ethene-1-sulfonamide (Pro-AVSN). In a 10 mL conical flask, protected Pro-AVSN **S8** (9.2 mg, 0.0138 mmol, 1.0 equiv.) was dissolved in 1 mL H_2O and cooled to 0 °C. TFA (1 mL) was added and stirring continued at 0 °C for 3 h. The vessel was warmed to 21 °C and stirring was continued for 5 h. TFA and water were removed by azeotroping the mixture in cyclohexane (3x4 mL), MeOH (3x4 mL), and benzene (3x4 mL). Purification by semi-preparative HPLC (C_{18}; 10 x 250 mm; gradient 5-95% CH_3CN in H_2O with 0.05% TFA over 30 min; 5 mL/min) afforded Pro-AVSN (5.9 mg, quant.) as a white solid.
^{1}H-NMR (400 MHz, CD_3OD): δ 8.39 (s, 1H), 8.33 (s, 1H), 6.86–6.70 (m, 2H), 5.99 (d, *J* = 5.8 Hz, 1H), 4.76 (t, 2H), 4.35 (t, 1H), 4.29 (q, *J* = 15.8, 7.2 Hz, 1H), 4.25–4.20 (m, 1H), 3.43–3.35 (m, 3H), 2.38–2.27 (m, 1H), 2.20–2.02 (m, 2H), 1.95–1.83 (m, 1H).

B. Protein expression and preparation of *holo*-PltL and PltF

B.1. Expression and purification of *holo*-PltL

The pET22b-PltL plasmid and the pREP4-sfp plasmid were obtained from the laboratory of Christopher Walsh at Harvard University. Both plasmids were co-transformed into *Escherichia coli* BL21 cells. The BL21 cells were grown in Luria-Bertani (LB) media with 50 µg/mL kanamycin and 100 µg/mL ampicillin. Expression was induced with 0.5 mM isopropyl β-D-1-

thiogalactopyranoside (IPTG) at an OD_{600} of 0.6. The cells were grown for at 25 °C for 16 hours, then harvested at 2500 relative centrifugal force (RCF). The pelleted cells were resuspended in 30 mL of 150 mM NaCl, 50 mM Tris pH7.5, 10% glycerol, 0.25 mg/mL lysozyme. The cells were further lysed with the Ultrasonic Processor FS-600N. The lysate was centrifuged at 12000 RCF for 1 hour and the supernatant was passed through the Novagen Ni-NTA resin column. *holo*-PltL was eluted with 15 mL of 150 mM NaCl, 50 mM Tris pH 7.5, 10% glycerol, and 250 mM imidazole. The expressed sfp did not have a his-tag and was did not bind to the column well. The eluant was passed through a Superdex S75 16/600 pg size exclusion column on an AKTA Pure fast performance liquid chromatography (FPLC) with 20 mM Tris pH 7.5 and 20 mM NaCl. The fractions containing *holo*-PltL were collected and concentrated to a final concentration of 2.2 mg/mL.

B.2. Expression and purification of PltF

The pET37b-PltF plasmid was obtained from the laboratory of Christopher Walsh at Harvard University. The plasmid was transformed into *E. coli* BL21 cells. The cells were grown in LB media with 50 µg/mL kanamycin. Expression was induced with 0.5 mM IPTG at an OD_{600} of 0.6. The cells were grown at 16 °C for 16 hours then harvested at 2500 relative centrifugal force (RCF). The pelleted cells were resuspended in 30 mL of 150 mM NaCl, 50 mM Tris pH 7.5, 10% glycerol, 0.25 mg/mL lysozyme. The cells were further lysed with the Ultrasonic Processor FS-600N. The lysate was centrifuged at 12000 RCF for 1 hour and the supernatant was passed through the Novagen Ni-NTA resin column. PltF was eluted with 15 mL of 150 mM NaCl, 50 mM Tris pH 7.5, 10% glycerol, and 250 mM imidazole. The eluant was passed through a Superdex S200 16/600 pg size exclusion column on an AKTA Pure FPLC with 20 mM Tris pH 7.5 and 20 mM NaCl. The fractions containing PltF were collected and concentrated to a final concentration of 30 mg/mL.

C. X-ray crystallography studies

C.1. Trapping of *holo*-PltL with PltF

In 30 uL, the trapping reaction between *holo*-PltL and PltF consisted of 30 mM Tris pH 7.5, 2.0 mM $MgCl_2$, 2.0 mM tris(2-carboxyethyl)phosphine (TCEP), 0.02% Triton X, 0.34 mM Pro-AVSN, 0.17 mM *holo*-PltL, and 0.17 mM PltF. The reaction was incubated for 24 hours at 4 °C prior to crystallization experiments.

C.2. Crystallization of the PltL-PltF complex

Initial crystallization conditions were identified by the Index high throughput sparse matrix screen from Hampton Research through hanging drop vapor diffusion. The initial condition included a 200 nL drop volume with a 1:1 ratio of 0.17 mM PltL-PltF (11 mg/mL) complex to 3.5 M sodium formate pH 7.0. Subsequent optimizations led to a crystal condition consisting of 400 nL drop volume with a 1:1 ratio of 0.17 mM PltL-PltF (11 mg/mL) complex to a solution of 3.18 M sodium formate and 0.1 M malonic acid pH 5.73. Single crystals were transferred into cryoprotectant consisting of 20% glycerol and 80% of the crystallization condition and immediately frozen in liquid nitrogen.

C.3. Data collection and structure determination

X-ray diffraction data were collected at the Advanced Light Source beam line 8.3.1 at the Lawrence Berkeley National Laboratory at a temperature of 110 K with a wavelength of 1.12 Å. The data was processed with XDS (4) and an initial structure was built using molecular replacement with MOLREP (5) using PDB ID 3E7W (6) as the search model for PltF. The structure was iteratively refined via automated refinement with REFMAC (7) and manual refinement with COOT (8). Then, PDB ID 2N5H (9) was used as a search model for the second round of molecular replacement to identify PltL. Then the Ppant/Pro-AVSN ligand and waters were added. The

coordinates and structure factor amplitudes were deposited in the Protein Data Bank with the accession code 6O6E.

D. Interface analysis

Protein Interfaces, Surfaces, and Assemblies (PISA) (10) from the European Bioinformatics Institute, in combination with manual identification, was used to identify the residues involved in the PCP-A domain interface. PISA was also used to calculate the protein-protein interface areas of each PCP-A domain interface and the *E. coli* AcpP-partner protein interface.

The NRPS PCP-A domain interfaces under comparison include the PltL-PltF complex in this study, the type II EntE-EntB complex (PDB ID 3RG2) (11), the type II didomain PA1221 (PDB ID 4DG9) (12), the type I LgrA (PDB ID 5ES8) (13), the type I EntF (PDB ID 5T3D) (14). The contribution of other proteins in the same complex for both type I systems were omitted in this analysis. The FAS AcpP-partner protein interfaces include the AcpP-FabA (PDB ID 4KEH) (15) and AcpP-FabZ complexes (PDB ID 6N3P) (16) (Figure S11).

E. Alignment and superposition of PltL structures

The “align” command in PyMol was used for sequence alignment, superposition, and refinement for aligning the structures of PltL (Figure S8). All 20 lowest energy solution NMR structures of *holo*-PltL (PDB ID 2N5H) were aligned to the bound state of PltL from the PltL-PltF crystal structure.

F. Mutagenesis of PltF

F.1. Preparation of PltF mutants

The PltF point mutations were introduced via QuikChange PCR (17). The primer sequences are listed in Figure S9. The PltF mutants were expressed and purified through the same methods as in B.2.

F.2. HPLC-based aminoacylation assay of PltF mutants

The aminoacylation reaction (30 uL) contained 50 mM Tris pH 7.5, 12.5 mM $MgCl_2$, 2.0 mM TCEP, 5 mM ATP, 5 mM L-Pro, 0.015 mM *holo*-PltL, and 0.27 uM PltF. Upon addition of ATP and L-Pro last, the reaction was mixed and incubated at 25 °C for 2 minutes. The reaction was quenched with 6 uL of formic acid and centrifuged for 10 minutes at 10,000 RCF. The supernatants were passed over the Ascentis Express Peptide ES-C18 column with solvent B for 2 minutes, then increasing 5-40% B over 8 minutes, and finally 40-44% over 10 minutes (Solvent A = H_2O, 0.05% trifluoroacetic acid (TFA); solvent B = acetonitrile, 0.05% TFA). Analyses were conducted on an Agilent HP 1100 series HPLC. The protein elution was monitored by absorbance at 210 nm (A_{210}) (Figure S5). The percent of *prolyl*- and *holo*-PltL was calculated through the integration of the chromatographic peak areas and using the A_{210} of *prolyl*-PltL divided by the summation of A_{210} of *prolyl*-PltL with A_{210} of *holo*-PltL. Each assay was performed in triplicate (Figure S10).

Table S2. Crystallography data.

PDB Entry	**6O6E**
	Data Collection
Space group	$P3_221$
***a, b,c* (Å)**	170.6, 170.6, 64.9
α, β, γ (deg)	90.0, 90.0, 120.0
resolution (Å)	2.14 (2.14-2.19)
total no. of reflections	59600
CC 1/2	98.9 (10.3)
I/σ(I)	9.73 (0.31)
Completeness	99.2 (90.5)
Redundancy	10.03 (8.48)
	Refinement
Resolution (Å)	2.14 (2.14-2.19)
No. of reflections	55985
R_{work}/R_{free}	0.216/0.261
No. of atoms (non-hydrogen)	
Protein	4354
Solvent	104
Heteroatoms	111
Average B factor (Å^2)	64.0
Ramachandran analysis (%)	
Favored	94.2
Allowed	5.5
Outliers	0.3
Root-mean-square deviation	
Bond lengths (Å)	0.009
Bond angles (°)	1.688

Numbers in parenthesis denotes highest resolution shell.

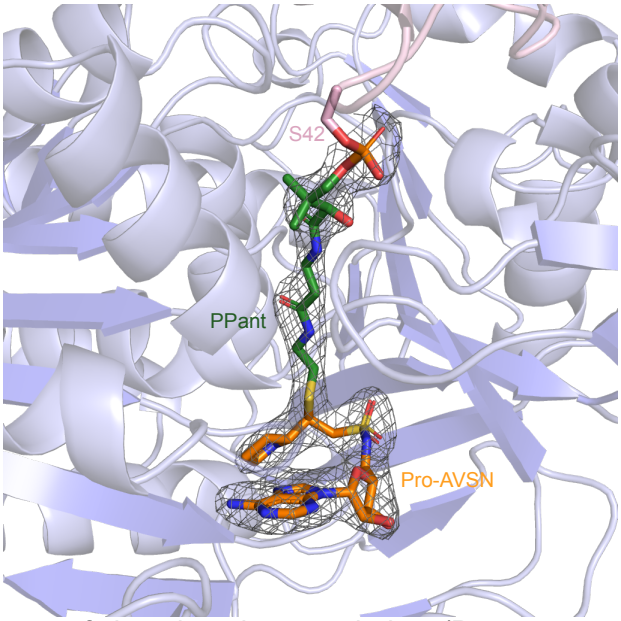

Figure S3. 2fo-fc omit map of the phosphopantetheine (Ppant, green) and prolyl-adenosine vinylsulfonamide (Pro-AVSN, orange). Electron density is contoured to 2σ (gray mesh).

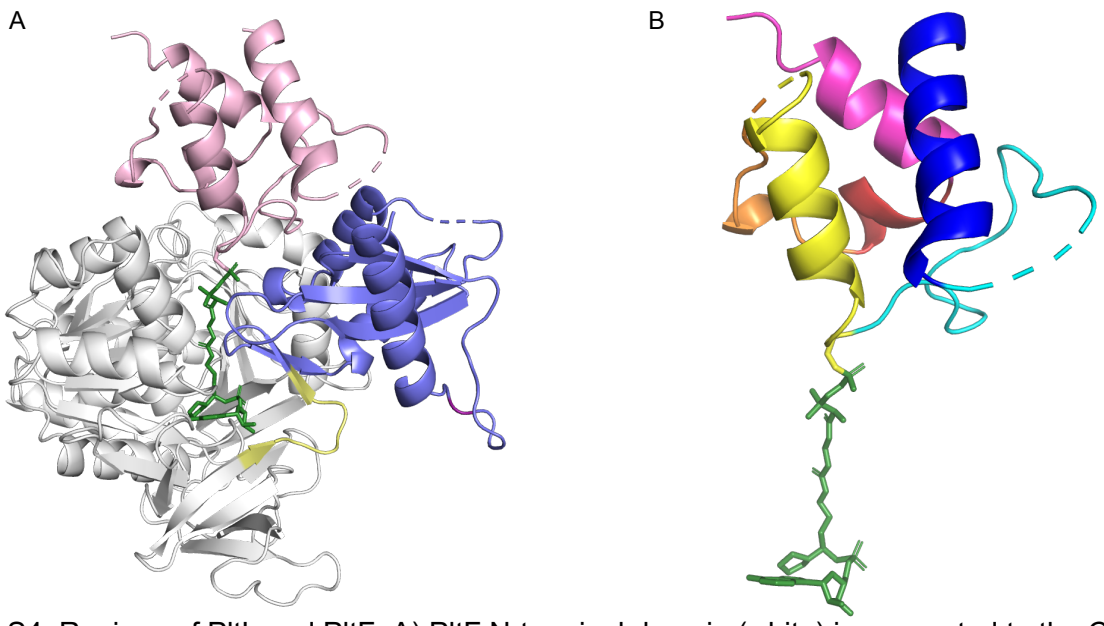

Figure S4. Regions of PltL and PltF. A) PltF N-terminal domain (white) is connected to the C-terminal domain (blue) via the hinge region (yellow). The catalytic K486 responsible for the adenylation reaction is shown in purple. B) The secondary structure of PltL are as follows: α helix 1 (residues 1-19, blue), loop 1 (residues 20-41, cyan), α helix 2 (residues 42-55, yellow), loop 2 (residues 56-61, orange), α helix 3 (residues 62-65, red), α helix 4 (residues 66-90, pink), phosphopantetheine and proline adenosine vinylsulfonamide (green).

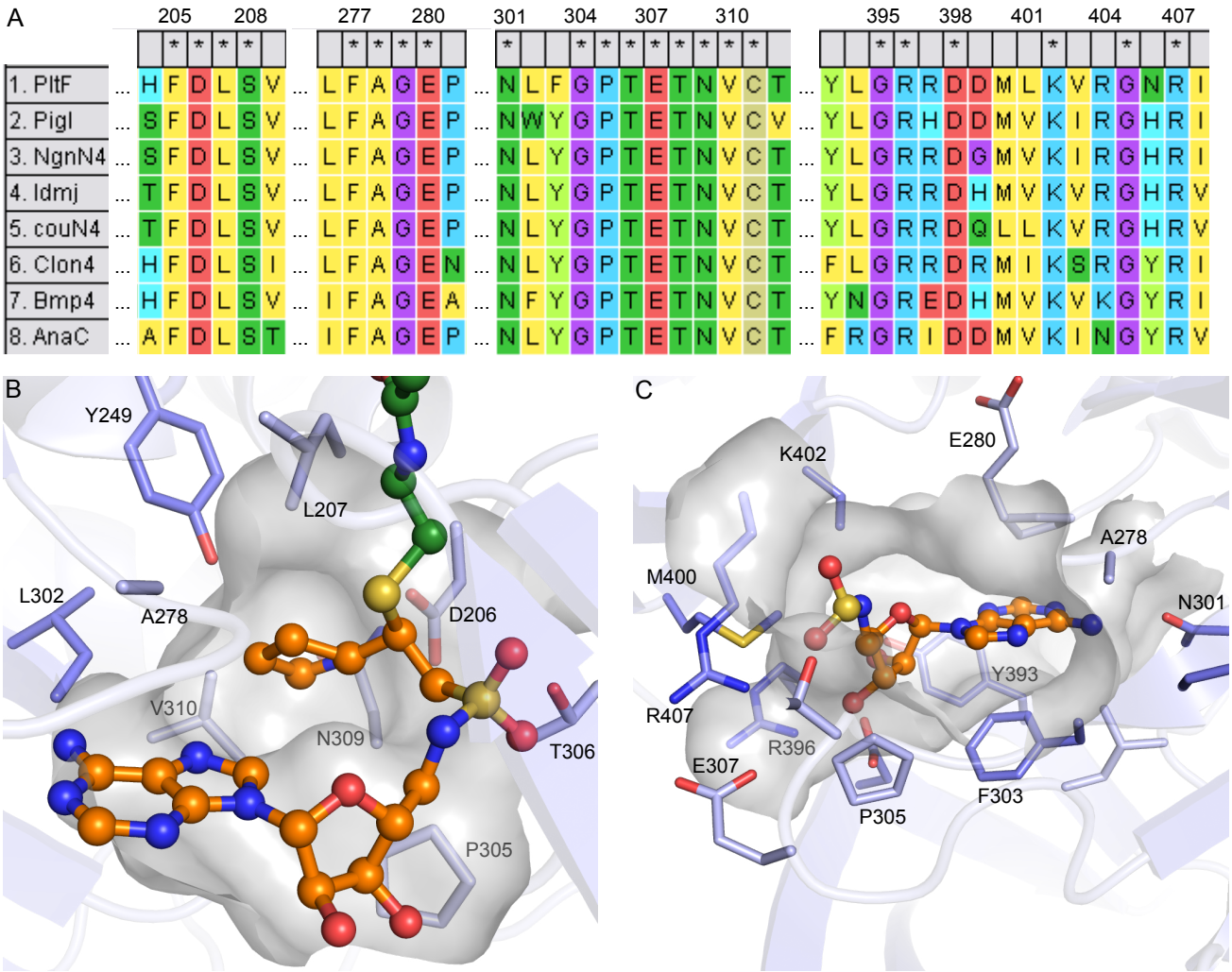

Figure S5. Conservation of the PltF active site. A) Highly conserved regions in proline-loading A domains are shown with an asterisk (*). These regions correspond to the L-proline binding site and the AMP binding site. B) Binding pocket of L-proline in PltF. C) Binding pocket of AMP in PltF. The Pro and Ppant moieties were excluded for clarity. The residues directly involved in forming the binding pocket are also found in the conserved regions from panel A.

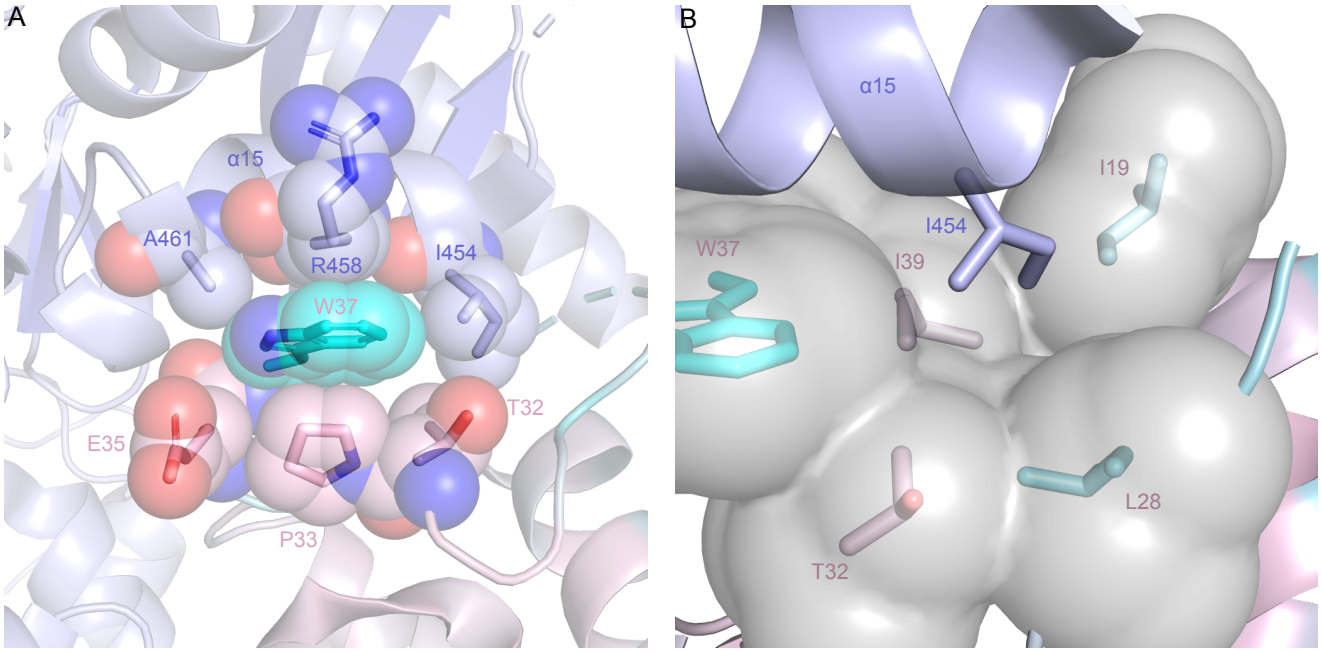

Figure S6. Interface hydrophobic interactions involving PltL Trp37. A) Burial of the indole ring of PltL Trp37 between PltF helix 15 and PltL loop 1 residues. The spheres represent van der waals radius of each atom. B) Close up of the surface of the PltL hydrophobic pocket that is occupied by PltF Ile454.

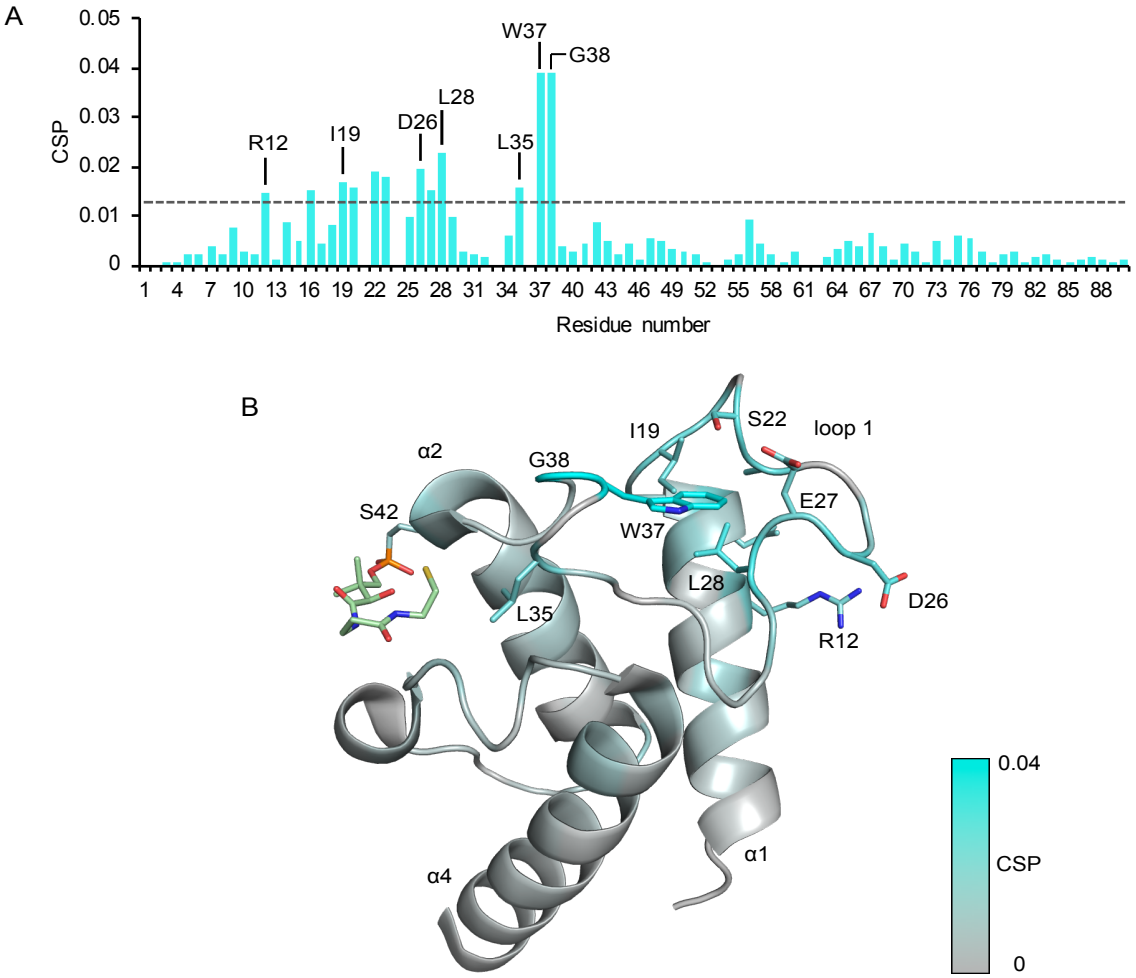

Figure S7. NMR studies of PltL from Jaremko et. al. 2017. A) Plot of the chemical shift perturbations of an NMR titration with an ^{15}N-labeled PltL with increasing equivalents of PltF. The dotted line indicates one standard deviation above the mean. The corresponding residue to each perturbation is listed on the x-axis. B) Solution NMR structure of *holo*-PltL with the CSPs from A) mapped on the model. The Ppant arm was also ^{15}N labeled upon HSQC peak identification.

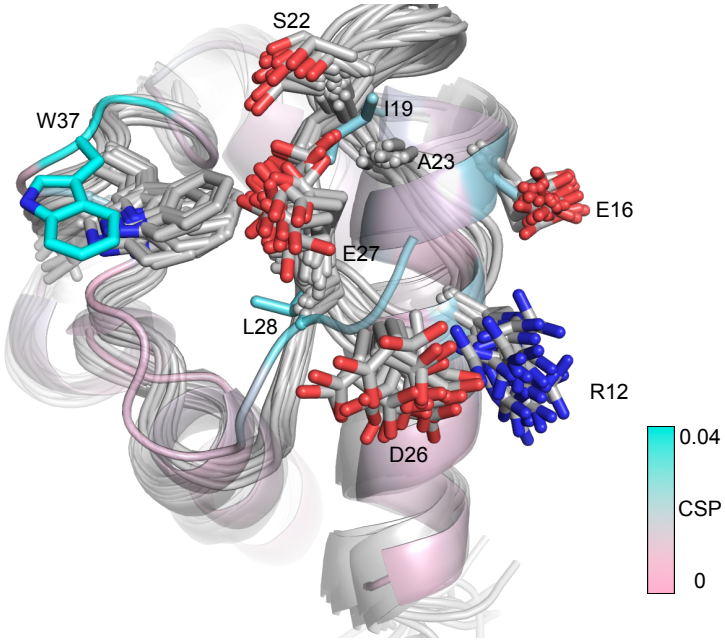

Figure S8. Superposition of the bound state of PltL (this study) with the solution NMR structures of unbound PltL (PDB ID 2N5H). The 20 lowest energy models of the PltL solution NMR structure (gray) was aligned to PltL (pink) in the bound state. The residues with high CSPs are shown; a change in intraprotein loop and side chain interactions correlates with the high CSPs. This alignment also highlights the required dynamical movement of PltL W37 upon binding to PltF.

Table S9. Primers for PltF mutant generation.

PltF Mutants	Forward Primer	Reverse Primer
F231A	CGCTGCATCGCCGCGGCTGCTGAC	CGATGCAGCGATCGACTCGGGAACCAGG
S232A	GTTCGCACCGCGGCTGCTGACCGACTT	CGGTGCGAACGCGATCGACTCGGGAAC
I454A	GCTGGCAGACCTCAAGCGCCACTGCG	GTCTGCCAGCGAAAGAGCGTCCCGGGT
K457A	CTCGCACGCCACTGCGCCCAGCG	CTCGCACGCCACTGCGCCCAGCG

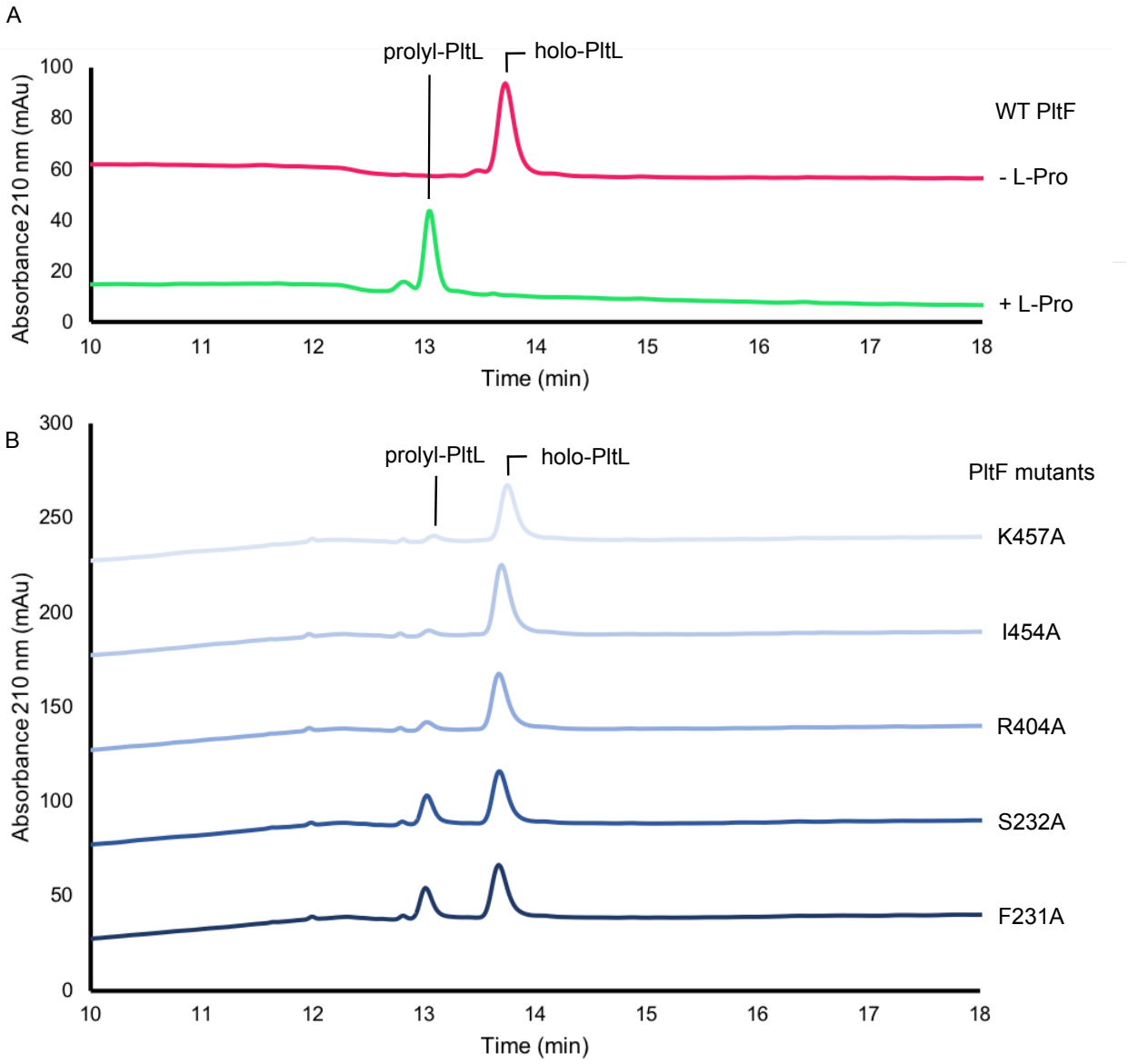

Figure S10. HPLC chromatograms of the aminoacylation of PltL by wild-type (WT) PltF and PltF mutants.

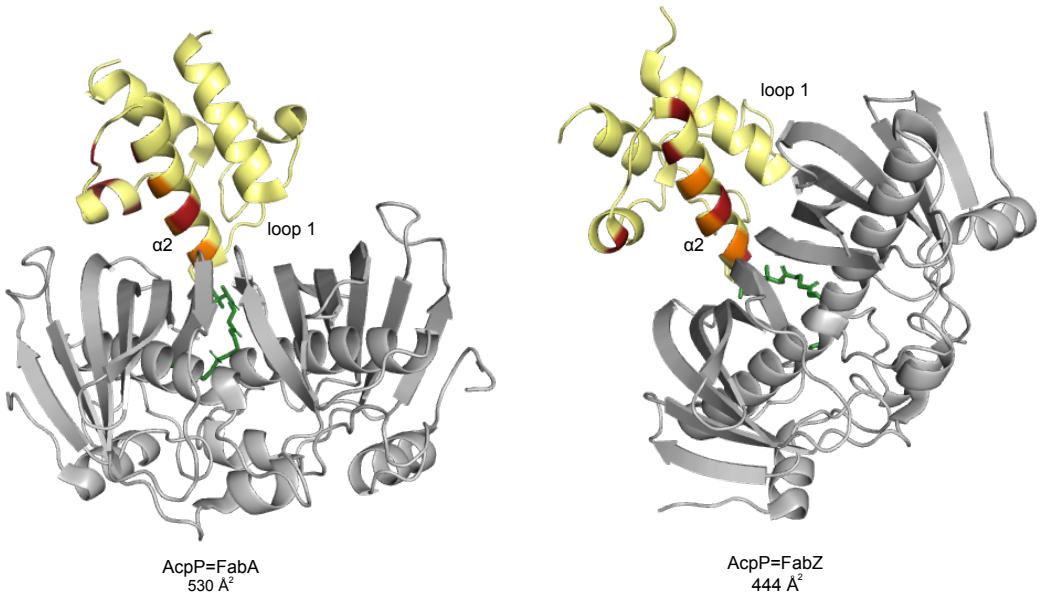

Figure S11. AcpP (yellow) interactions with its partner proteins (gray) in *E. coli* fatty acid biosynthesis. The protein-protein interface interactions of AcpP=FabA (left, PDB ID 4KEH) and of AcpP=FabZ (right, PDB ID 6N3P) consist of hydrophobic and salt bridge interactions and are almost exclusively located in alpha helix 2 of AcpP. The interface area was calculated, and protein-protein interactions identified via PISA. The interface areas of PCP-A domain interfaces are as follows: PltL-PltF 847 Å^2, EntE-EntB 928 Å^2, PA1221 675 Å^2, EntF 731 Å^2, LgrA 662 Å^2.

1H-NMR (400 MHz) of Weinreb amide S1 in CDCl3

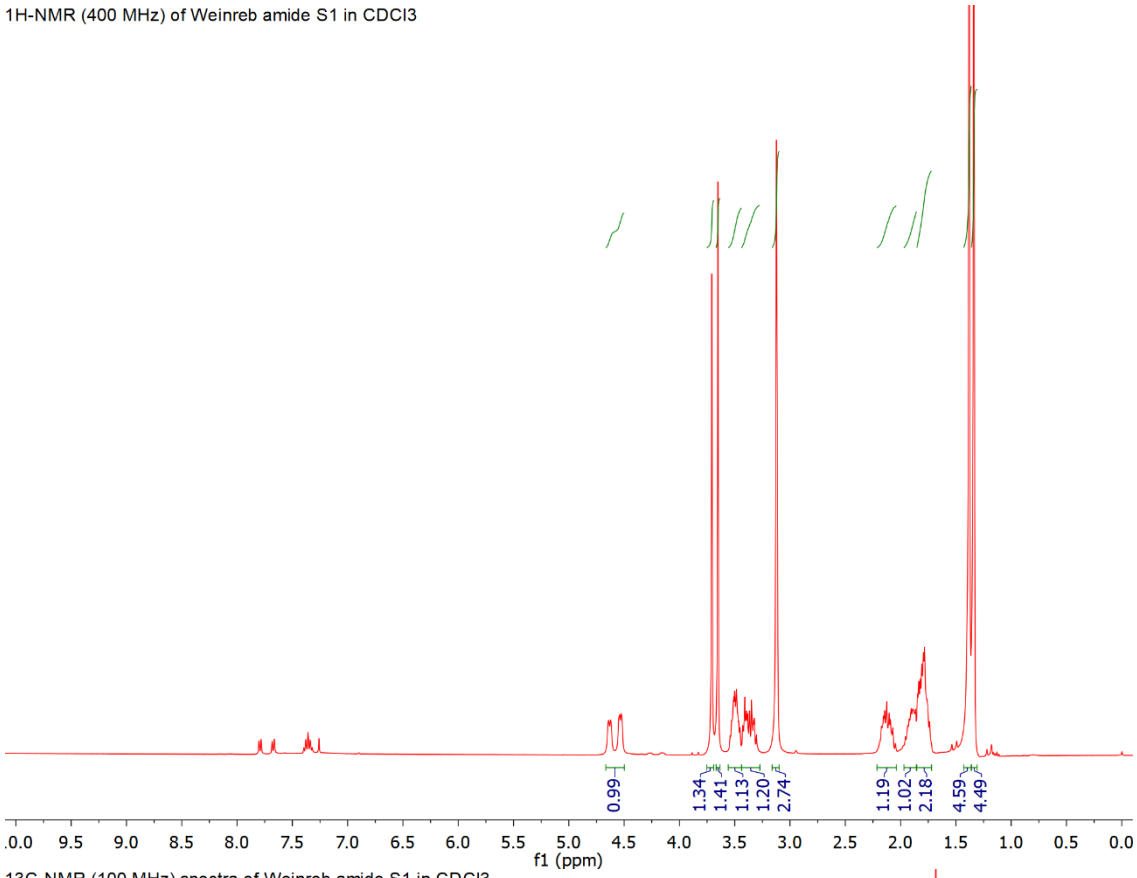

13C-NMR (100 MHz) spectra of Weinreb amide S1 in CDCl3

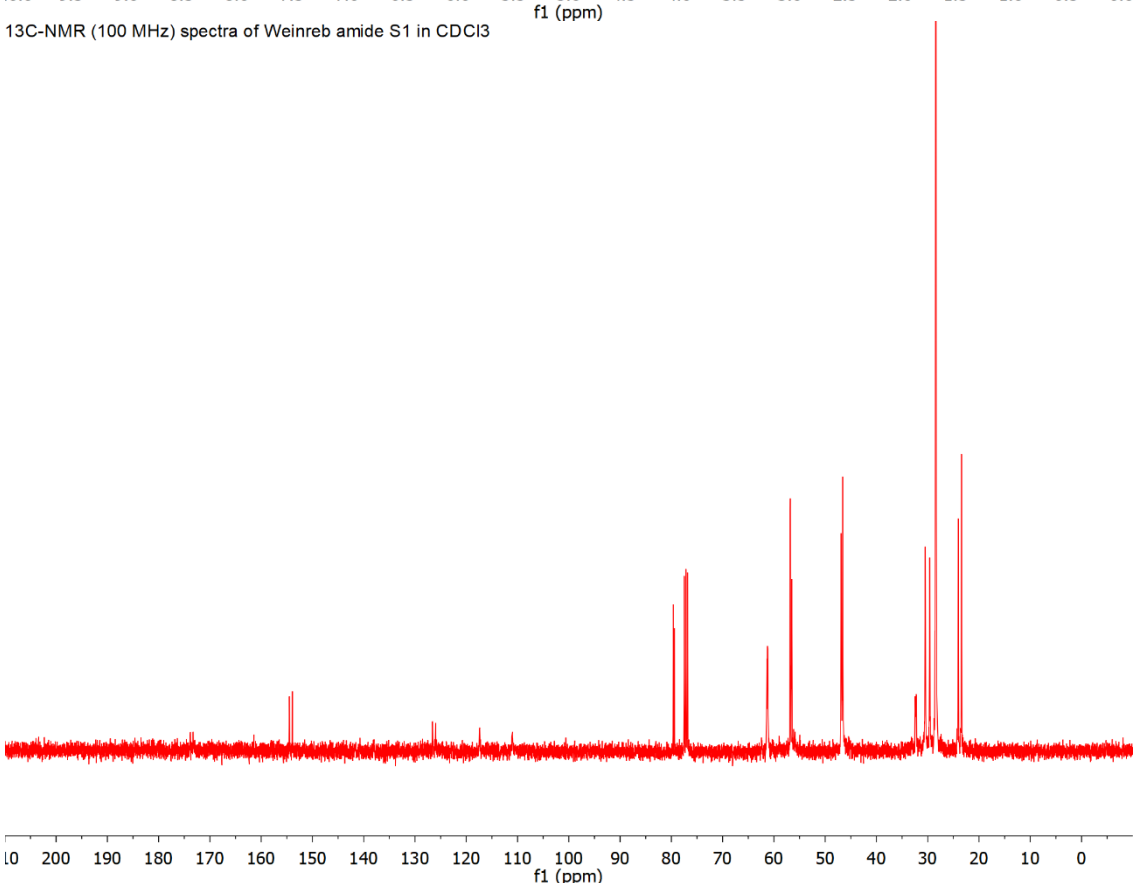

1H NMR (400 MHz) of aldehyde S2 in CDCl3

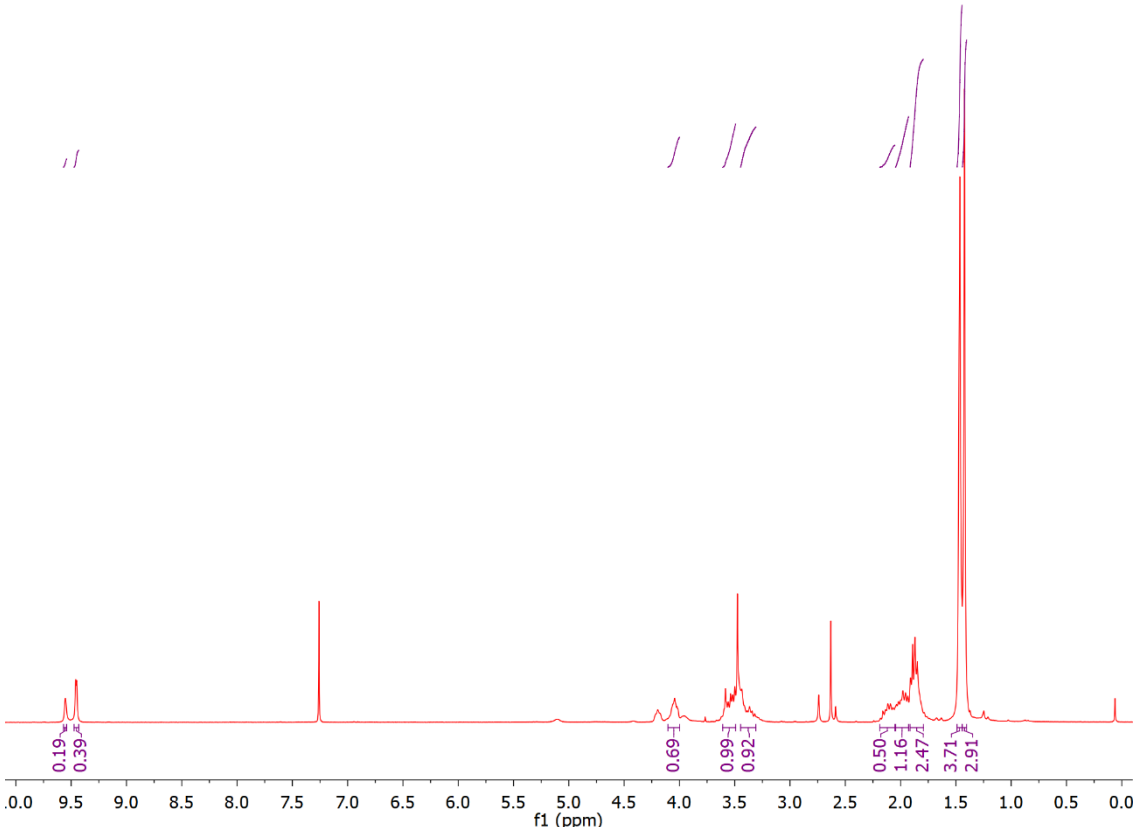

1H NMR (400 MHz) of ethyl vinyl sulfonate S4 in CDCl3

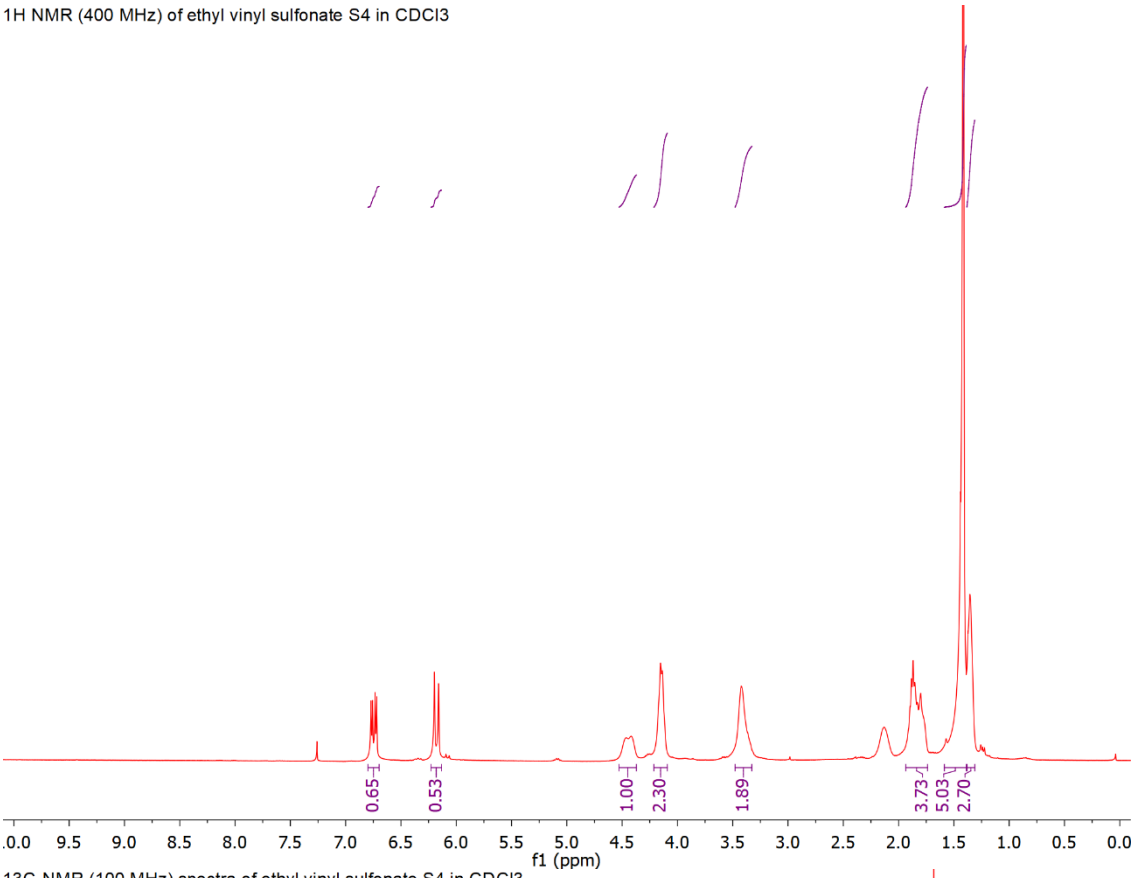

13C-NMR (100 MHz) spectra of ethyl vinyl sulfonate S4 in CDCl3

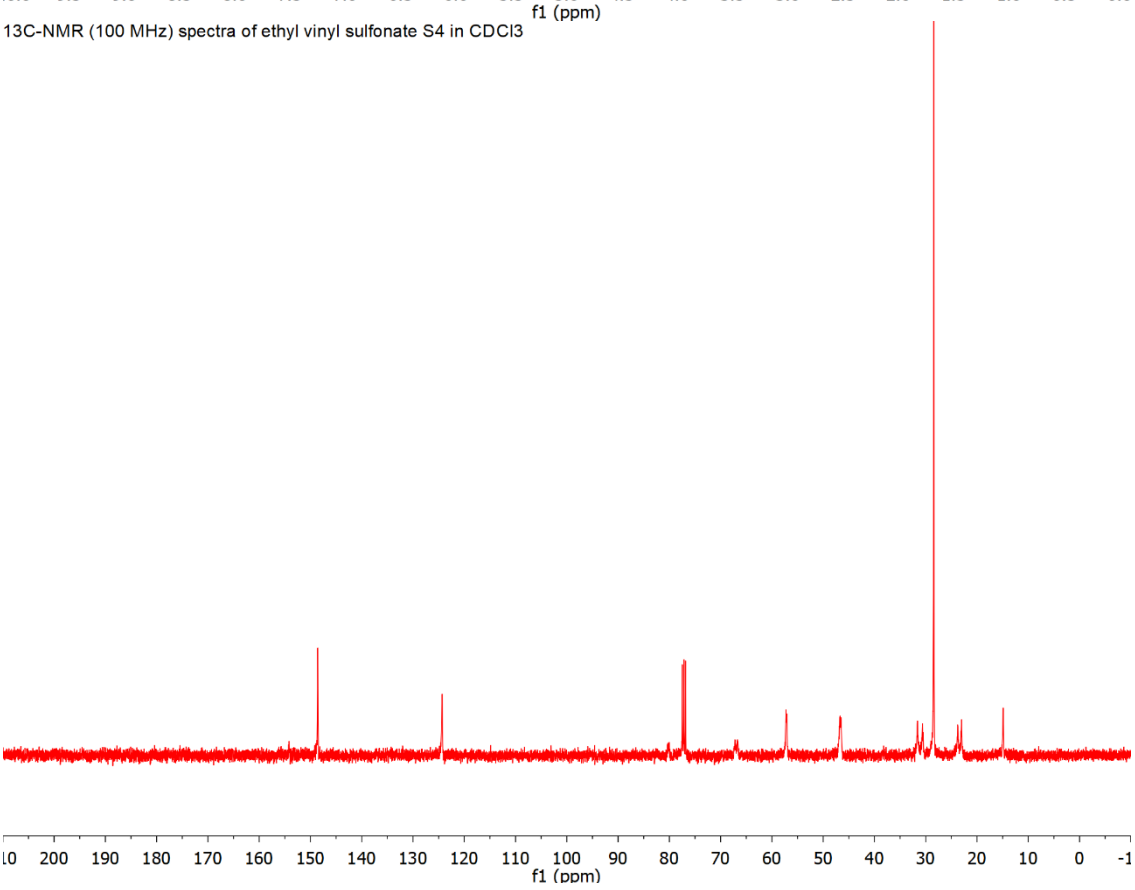

1H-NMR (400 MHz) of vinyl sulfonyl chloride S6 in CDCl3

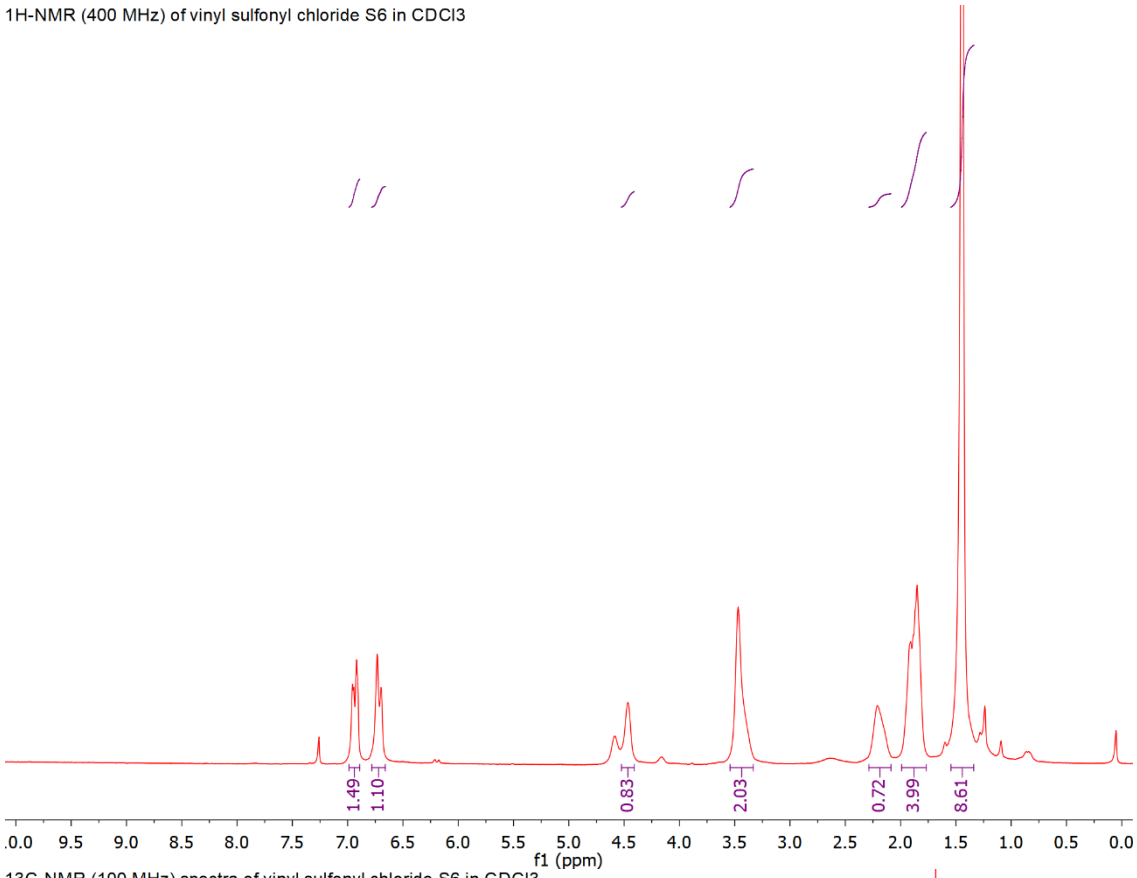

13C-NMR (100 MHz) spectra of vinyl sulfonyl chloride S6 in CDCl3

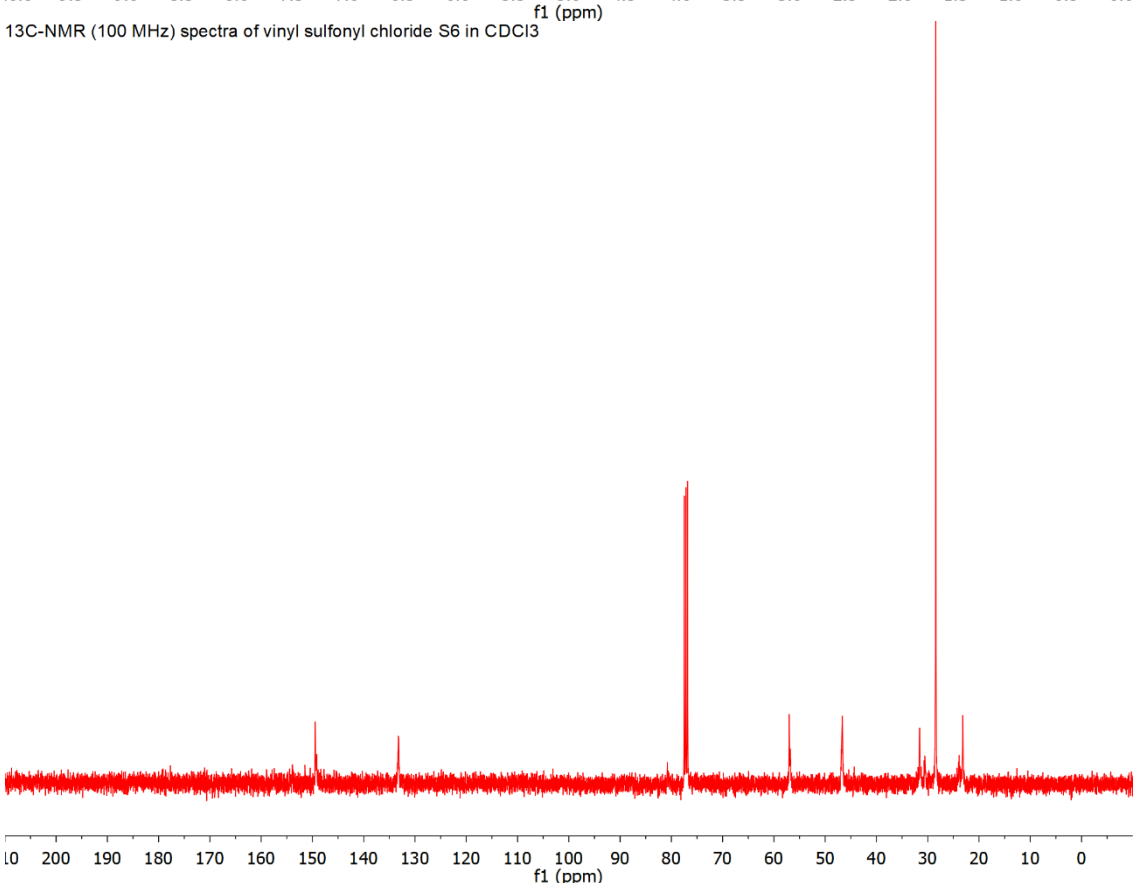

1H NMR (500 MHz) Boc-Pro-AVSN S8 in CDCl3

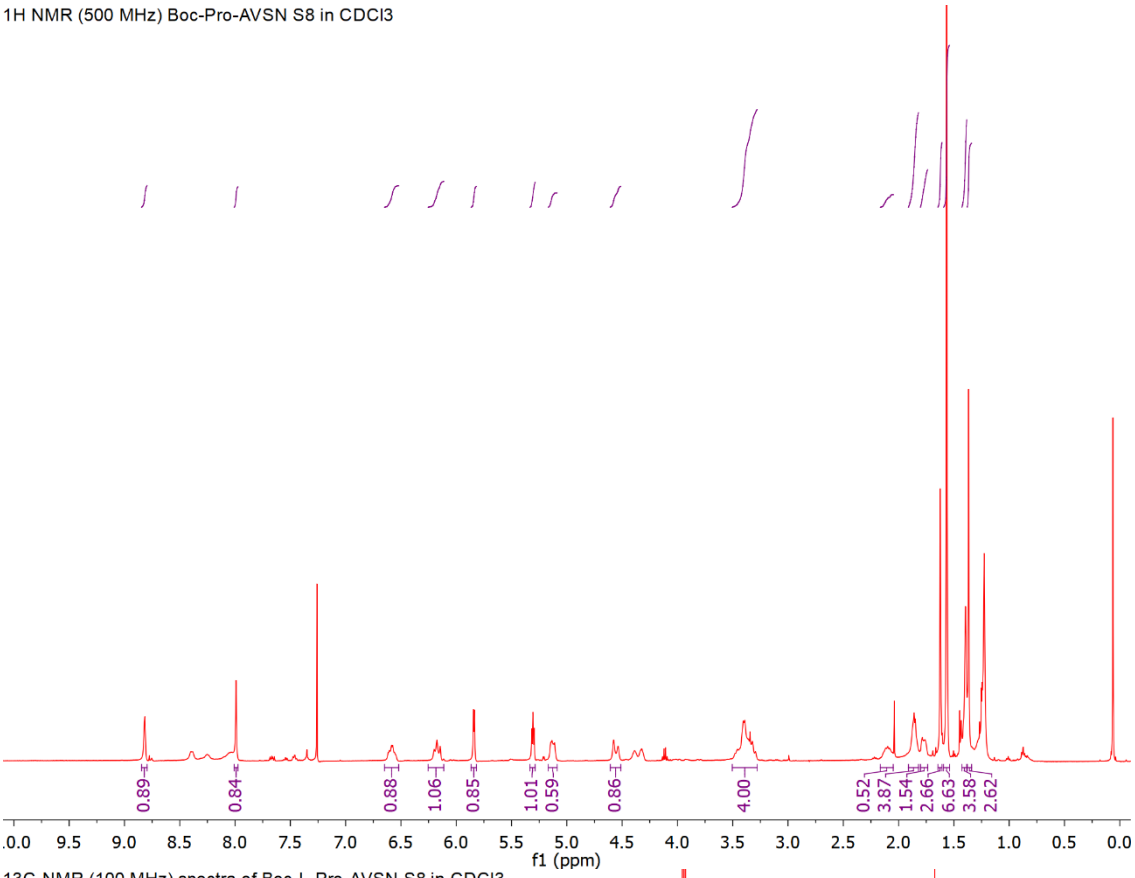

13C-NMR (100 MHz) spectra of Boc-L-Pro-AVSN S8 in CDCl3

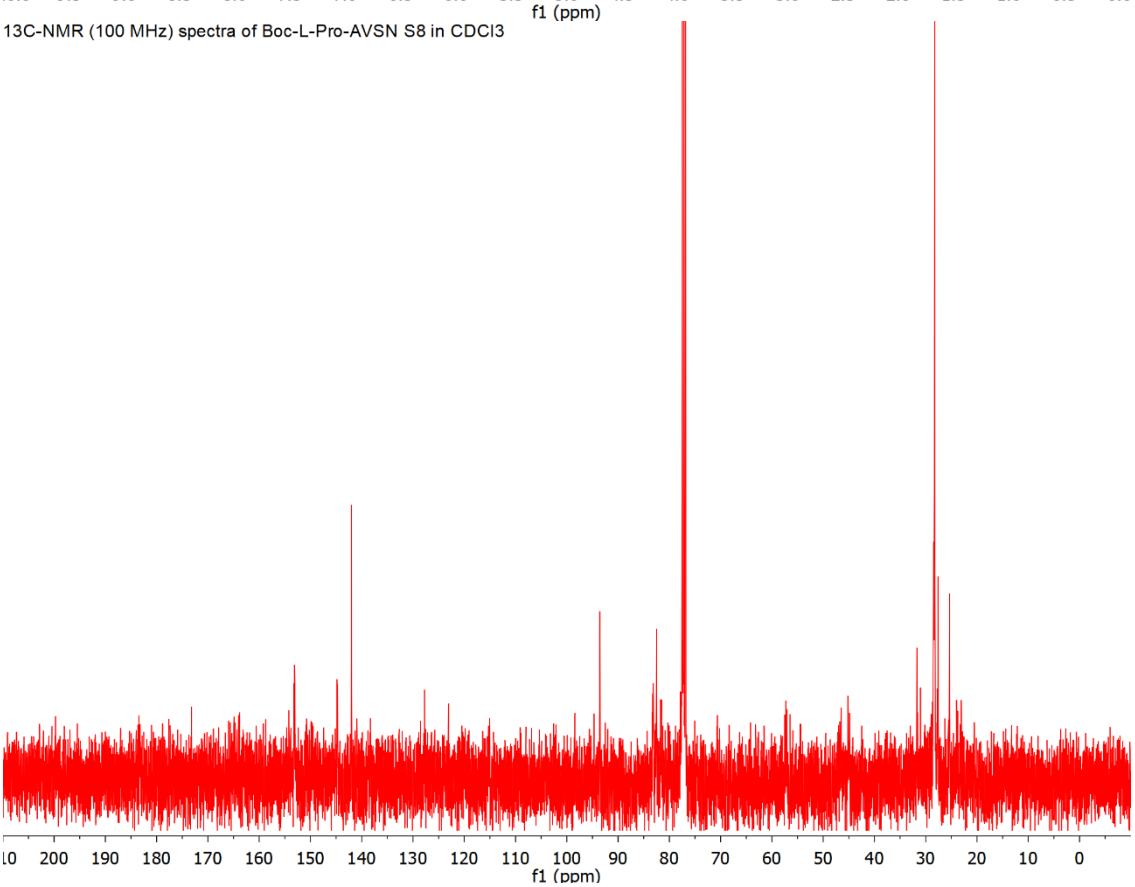

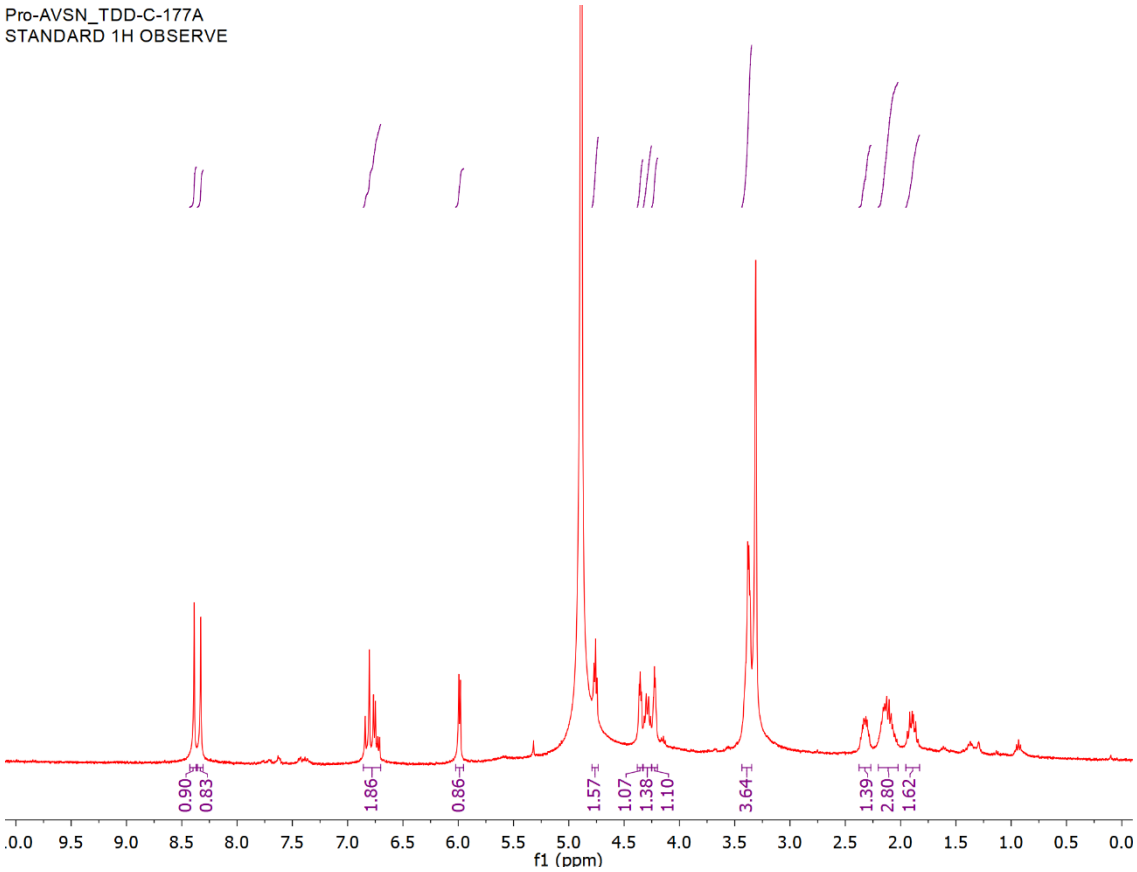
Pro-AVSN_TDD-C-177A
STANDARD 1H OBSERVE
0.90
0.83
1.86
0.86
1.57
1.07
1.38
1.10
3.64
1.39
2.80
1.62
.0.0 9.5 9.0 8.5 8.0 7.5 7.0 6.5 6.0 5.5 5.0 4.5 4.0 3.5 3.0 2.5 2.0 1.5 1.0 0.5 0.0
f1 (ppm)

G. SI References

1. Gottlieb HE, Kotlyar V, Nudelman A. NMR Chemical Shifts of Common Laboratory Solvents as Trace Impurities. J Org Chem. 1997 Oct;62(21):7512–5.

2. Carretero JC, Oemillequand M. SYNTHESIS OF a,B-UNSATURATED SULPHONATES VIA THE WITTIG-HORNER REACTION. :10.

3. Lu X, Zhang H, Tonge PJ, Tan DS. Mechanism-based inhibitors of MenE, an acyl-CoA synthetase involved in bacterial menaquinone biosynthesis. Bioorg Med Chem Lett. 2008 Nov;18(22):5963–6.

4. Kabsch W. *XDS*. Acta Crystallogr D Biol Crystallogr. 2010 Feb 1;66(2):125–32.

5. Vagin A, Teplyakov A. *MOLREP* : an Automated Program for Molecular Replacement. J Appl Crystallogr. 1997 Dec 1;30(6):1022–5.

6. Yonus H, Neumann P, Zimmermann S, May JJ, Marahiel MA, Stubbs MT. Crystal Structure of DltA: IMPLICATIONS FOR THE REACTION MECHANISM OF NON-RIBOSOMAL PEPTIDE SYNTHETASE ADENYLATION DOMAINS. J Biol Chem. 2008 Nov 21;283(47):32484–91.

7. Murshudov GN, Vagin AA, Dodson EJ. Refinement of Macromolecular Structures by the Maximum-Likelihood Method. Acta Crystallogr D Biol Crystallogr. 1997 May 1;53(3):240–55.

8. Emsley P, Cowtan K. *Coot* : model-building tools for molecular graphics. Acta Crystallogr D Biol Crystallogr. 2004 Dec 1;60(12):2126–32.

9. Jaremko MJ, Lee DJ, Opella SJ, Burkart MD. Structure and Substrate Sequestration in the Pyoluteorin Type II Peptidyl Carrier Protein PltL. J Am Chem Soc. 2015 Sep 16;137(36):11546–9.

10. Krissinel E, Henrick K. Inference of Macromolecular Assemblies from Crystalline State. J Mol Biol. 2007 Sep;372(3):774–97.

11. Sundlov JA, Shi C, Wilson DJ, Aldrich CC, Gulick AM. Structural and Functional Investigation of the Intermolecular Interaction between NRPS Adenylation and Carrier Protein Domains. Chem Biol. 2012 Feb;19(2):188–98.

12. Mitchell CA, Shi C, Aldrich CC, Gulick AM. Structure of PA1221, a Nonribosomal Peptide Synthetase Containing Adenylation and Peptidyl Carrier Protein Domains. Biochemistry. 2012 Apr 17;51(15):3252–63.

13. Reimer JM, Aloise MN, Harrison PM, Martin Schmeing T. Synthetic cycle of the initiation module of a formylating nonribosomal peptide synthetase. Nature. 2016 Jan;529(7585):239–42.

14. Drake EJ, Miller BR, Shi C, Tarrasch JT, Sundlov JA, Leigh Allen C, et al. Structures of two distinct conformations of holo-non-ribosomal peptide synthetases. Nature. 2016 Jan;529(7585):235–8.

15. Nguyen C, Haushalter RW, Lee DJ, Markwick PRL, Bruegger J, Caldara-Festin G, et al. Trapping the dynamic acyl carrier protein in fatty acid biosynthesis. Nature. 2014 Jan;505(7483):427–31.

16. Dodge GJ, Patel A, Jaremko KL, McCammon JA, Smith JL, Burkart MD. Structural and dynamical rationale for fatty acid unsaturation in *Escherichia coli*. Proc Natl Acad Sci. 2019 Apr 2;116(14):6775–83.

17. Liu H, Naismith JH. An efficient one-step site-directed deletion, insertion, single and multiple-site plasmid mutagenesis protocol. BMC Biotechnol. 2008;8(1):91.